

1 Vision

1.1 Overview

Localisation and Image Analysis: A fundamental challenge in image analysis is the localisation problem: detecting areas over which large signals have occurred. This issue is encountered in various fields including geostatistical disease mapping, neuroimaging, and cosmology, where research questions include “Where does observed malaria prevalence indicate an outbreak?” and “Where do changes in blood flow in the brain occur in response to a task?”. Formally, the localisation problem seeks to estimate spatial regions over which a signal, μ , exceeds a threshold c . Despite the spatial nature of the problem, existing methods give little consideration to the random topological and geometric properties of such regions. Here, we address this issue by proposing novel statistical methods that explicitly account for and model such properties.

This proposal centers primarily on fMRI neuroscience, in which lattice data is observed over a compact C^1 manifold $S \subset \mathbb{R}^N$ representing, for instance, an entire brain volume or a smooth cortical surface. The primary aim of fMRI analysis is to identify brain regions that are active under a particular task [26, 13, 30, 36, 66] or to detect differences in brain function between groups of subjects [52, 51]. At times, we shall also consider a secondary application of disease prevalence studies. In this setting, S represents a geographical region over which data has been irregularly sampled, and, to inform public health policy, the aim is to identify spatial regions at which a disease prevalence exceeds a predefined threshold [31, 20].

The signal plus noise model: We assume a *signal plus noise* model, defined for spatial locations $s \in S$ as:

$$\hat{\mu}(s) = \mu(s) + \epsilon(s). \quad (1)$$

Here, $\mu \in C^1(S, \mathbb{R})$ is the spatially varying signal of interest, $\hat{\mu}$ is an almost surely (a.s.) C^1 estimate of μ derived from n samples, and ϵ is the error term. The point-wise standard deviation of ϵ is denoted $\sigma \in C^1(S, \mathbb{R}^+)$. We also assume a functional CLT of the form:

$$\hat{G} := \frac{\hat{\mu} - \mu}{\hat{\sigma}/\sqrt{n}} \xrightarrow{d} G, \quad (2)$$

where $\hat{\sigma}$ is a consistent estimator of σ and G is a.s. C^1 . Our interest lies in excursion sets of the form $\mathcal{A}_c := \{s \in S : \mu(s) \geq c\}$, and their estimates $\hat{\mathcal{A}}_c := \{s \in S : \hat{\mu}(s) \geq c\}$ (Fig. 1 Panel (a)). When μ exceeds c at a given location, we describe that location as being “active”.

Our approach differs from the existing literature in two fundamental ways. First, we focus on the connected components or ‘clusters’ within \mathcal{A}_c , whereas current work only provides statements about the *excursion set as a whole* ([27, 4, 63]). While a seemingly fine distinction, the practical interpretation of spatial signal crucially depends on interpretation of individual components and, in neuroimaging in particular, “cluster inference” is the dominant approach to assessing signals in brain maps. Second, unlike existing approaches, which make restrictive assumptions of normality or stationarity on the noise or smoothness of the signal mean ([6, 22, 20]), our proposed theory requires no further assumption on either the point-wise distribution or the spatial covariance of ϵ or $\hat{\mu}$. To apply the theory in practice using bootstrap techniques, we additionally assume that G is symmetrically distributed.

Estimation via Spatial Information: fMRI analysis conventionally reports the ‘peaks’ of $\hat{\mu}$ and clusters of $\hat{\mathcal{A}}_c$ (Fig. 2), with the aim of identifying estimated clusters with anatomical regions. Many conventional analyses incorporate spatial information by treating small ‘clusters’ as false positives and removing them from consideration. A major drawback of this approach, known as ‘cluster-size’ infer-

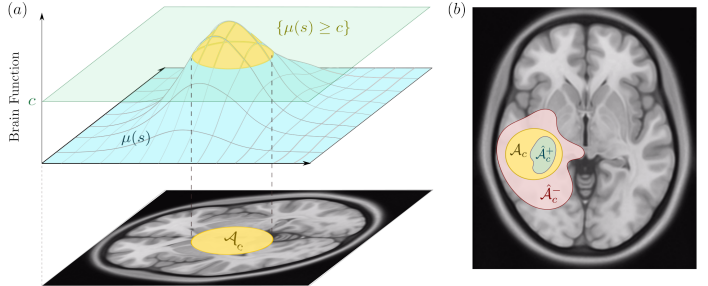


Fig. 1: An excursion set, \mathcal{A}_c , representing a region of brain activation in fMRI. Panel (a): Illustration of how the excursion set, \mathcal{A}_c , is derived from the function $\mu(s)$. Panel (b): Confidence regions, $\hat{\mathcal{A}}_c^+$ and $\hat{\mathcal{A}}_c^-$, providing conservative and liberal confidence bounds on the location of \mathcal{A}_c , shown in blue and red, respectively.

ence is that, when a cluster is declared significant, the strongest statement that can be inferred is “*at least one voxel (3D pixel) in the cluster was truly active*”. For large clusters, this statement is imprecise and lacks interpretability. In response, recent work has introduced the True Discovery Proportion (TDP) ([9, 14]). For each cluster estimate $\hat{\mathcal{K}}_c$, the TDP is the *expected percentage* of $\hat{\mathcal{K}}_c$ that is “truly” active; $TDP = \mathbb{E}[|\hat{\mathcal{K}}_c \cap \mathcal{A}_c|/|\hat{\mathcal{K}}_c|]$. Existing TDP methods utilize closed testing procedures but do not incorporate spatial information ([32]).

Assessing Spatial Uncertainty: Uncertainty estimates in fMRI are available for *signal magnitude*, but not for *cluster location*. To address this, recent efforts have introduced Confidence Regions (CRs) for an excursion set \mathcal{A}_c . CRs are binary sets, $\hat{\mathcal{A}}_c^+$ and $\hat{\mathcal{A}}_c^-$, which satisfy $\mathbb{P}[\hat{\mathcal{A}}_c^+ \subseteq \mathcal{A}_c \subseteq \hat{\mathcal{A}}_c^-] = 1 - \alpha$ for a given confidence level α ([40, 10, 49]). If a pair of CRs closely resemble one another, then $\hat{\mathcal{A}}_c$ is deemed to be a reliable estimate of \mathcal{A}_c while a lack of resemblance indicates the need for more data. Following [54, 11, 12], we construct CRs as $\hat{\mathcal{A}}_c^\pm = \{s \in S : \frac{\hat{\mu}(s) - c}{\hat{\sigma}(s)/\sqrt{n}} \geq \pm q\}$ for a fixed quantile q . In [54], it was shown, under modest assumptions on the topology of μ at the level c , that:

$$\lim_{n \rightarrow \infty} \mathbb{P}[\hat{\mathcal{A}}_c^+ \subseteq \mathcal{A}_c \subseteq \hat{\mathcal{A}}_c^-] = \mathbb{P}\left[\sup_{s \in \partial\mathcal{A}_c} |G(s)| \leq q\right], \quad (3)$$

where $\partial\mathcal{A}_c := \{s \in S : \mu(s) = c\}$ is the boundary. In practice, q is estimated as the $(1 - \alpha)\%$ quantile of $\sup_{\partial\mathcal{A}_c} |G|$ via a wild t -bootstrap. Only the symmetry of G is assumed, with no further assumption on the distribution of $\sup_{\partial\mathcal{A}_c} |G|$.

Excursion Sets Framed as Clusters: Cluster-specific factors, such as cluster size, spatial correlation in the noise, and signal smoothness impact how easily the sampling characteristics of a cluster may be estimated. However, existing methods do not account for this complexity, often treating clusters as i.i.d. in order to draw inferences. Examples of this practice include [25], [35] and [53], each of which is implemented in at least one widely used fMRI analysis software package. Although these methods claim to make statements about individual ‘clusters’, the inference they provide utilizes only properties of the *excursion set as a whole*.

Convergence and Topology: Research questions in image analysis are often topological in nature, aiming to identify clusters or compare patterns of activation. To meaningfully address such questions it is imperative that the topological features of $\hat{\mathcal{A}}_c$ resemble, or converge to, those of \mathcal{A}_c . For instance, consider the Betti numbers $\{b_k(\mathcal{A}_c)\}$, which count the clusters, loops, and higher-dimensional ‘holes’ in a space (Fig. 3) ([64, 21]). Although it may seem intuitive that the estimated number of clusters, $b_0(\hat{\mathcal{A}}_c)$, ‘should’ converge to $b_0(\mathcal{A}_c)$, this is not always the case, especially in fields such as cosmology and material science, where \mathcal{A}_c can exhibit fractal-like behaviour ([3, 1, 28]). Identifying minimal conditions under which such convergence holds is crucial to interpreting the topological features of observed images.

Throughout this proposal, we assume a data resolution sufficient to capture the topological properties of \mathcal{A}_c and $\hat{\mathcal{A}}_c$. Our theory shall focus on their underlying representations in continuous space, while practical implementations shall consider discretized sets on a voxel lattice.

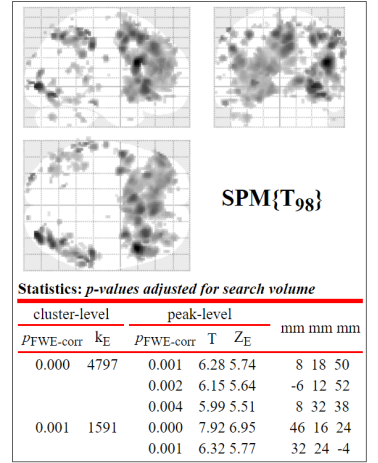


Fig. 2: Extract from conventional fMRI analysis results. Note that inference focuses on signal ‘peaks’ and ‘clusters’.

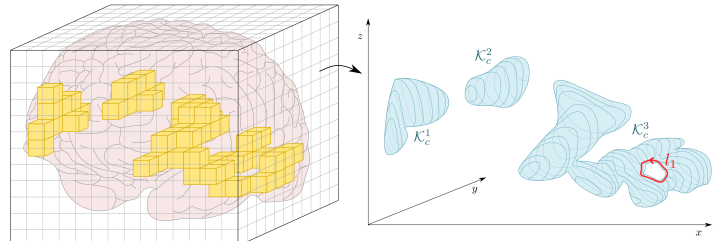


Fig. 3: Left: Discrete representation of $\hat{\mathcal{A}}_c$ on a voxel lattice. Right: $\hat{\mathcal{A}}_c$ represented in continuous space. $\hat{\mathcal{A}}_c$ has three clusters; K_c^1 , K_c^2 and K_c^3 , so $b_0(\mathcal{A}_c) = 3$. There is one non-trivial loop, l_1 , and thus $b_1(\mathcal{A}_c) = 1$. $b_2(\mathcal{A}_c) = 0$ as \mathcal{A}_c contains no 2-cycles, or ‘hollow’ regions.

Software and Real Data Analysis: All proposed methodology will be implemented as open-source user-friendly Python toolboxes for fMRI analysis. These toolboxes will be interoperable with large-scale data platforms previously developed by the PI such as the BLMM and crttoolbox packages ([47, 7, 49, 44, 46]). Further, to ensure correctness, in addition to extensive Monte Carlo simulations, all theory will be verified large-scale task-based fMRI datasets such as the UK Biobank (UKB) and Human Connectome Project (HCP) ([5, 61]).

1.2 Innovation

Although image analysis hinges on the interpretation of random clusters, current practice centers on the analysis of features of the excursion set in its entirety. This grant proposes a conceptual shift; to focus on the statistical properties of *individual clusters* rather than the excursion set as a whole.

To realize this shift, we shall first show that it does indeed make mathematical sense to investigate the properties of each cluster in isolation. Following this, we shall demonstrate, via rigorous proof, real data analysis and simulation, that making such a distinction can greatly improve the statistical power and interpretability of existing methods, such as TDP and CRs. Specifically, we propose:

- **Aim 1: Develop a rigorous, general theory of topological convergence.** Drawing upon techniques from differential topology, we derive minimal conditions for which topological invariants such as the Betti numbers of a random field converge. Practical methods are then proposed for assessing whether estimated clusters are truly ‘isolated’.
- **Aim 2: Derive an exact, local distribution for cluster size.** By applying the co-area formula from integral geometry and the multivariate delta method, we derive a novel central limit theorem for the distribution of cluster size. We apply this result to obtain a bound on the TDP and highlight potential applications for irregularly sampled data.
- **Aim 3: Enhance the specificity and interpretability of confidence regions.** By drawing upon notions of Skorokhod convergence from 2D financial analysis, we derive CRs for partitions of S in higher-dimensional settings. Utilising theory from Aim 1, we show that a special case of our derivations allows CRs to be generated for individual clusters and outline a practical method for doing so.

2 Approach

2.1 Aim 1: Cluster-wise Convergence

To make statements about individual clusters of \mathcal{A}_c , we must first establish theory relating the topology of $\hat{\mathcal{A}}_c$ to that of \mathcal{A}_c . Here, we shall identify the conditions under which the Betti numbers of $\hat{\mathcal{A}}_c$ converge to those of \mathcal{A}_c . It’s important to note that $\hat{\mathcal{A}}_c$ could display unpredictable patterns if such conditions aren’t met, even when working with large data sets. We conjecture the following:

Conjecture 1. If $\nabla\mu$ and $\nabla(\mu|_{\partial S})$ are non-zero on $\partial\mathcal{A}_c$, and both $\|\hat{\mu}_n - \mu\|_\infty$ and $\|\nabla\hat{\mu}_n - \nabla\mu\|_\infty$ tend to zero a.s., then $d_H(\hat{\mathcal{A}}_c, \mathcal{A}_c) \xrightarrow{a.s.} 0$ and, for every k , $b_k(\hat{\mathcal{A}}_c) \xrightarrow{a.s.} b_k(\mathcal{A}_c)$. Analogous statements hold for convergence in probability and distribution.

In the above, d_H denotes the Hausdorff distance. Initial derivations show Conjecture 1 holds for $k = 0$. Drawing upon techniques from differential geometry and topology, building on existing collaborations with Prof. Armin Schwartzman’s spatial statistics group at the University of California, we propose to show the above holds for all k , as well as for components of CRs. To be specific, we propose

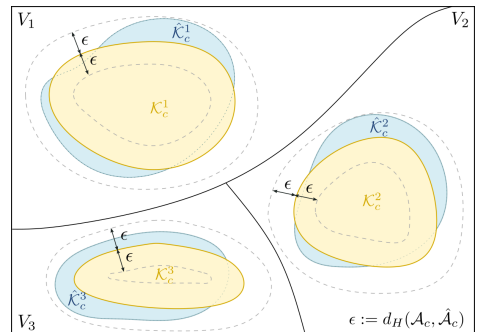


Fig. 4: The partition $\{V_i\}$ (solid black), which isolates clusters of \mathcal{A}_c (yellow), and clusters of $\hat{\mathcal{A}}_c$ (blue). Also shown are ϵ -tubes of width $d_H(\mathcal{A}_c, \hat{\mathcal{A}}_c)$ around \mathcal{A}_c (grey dashed).

that given $\hat{\mathcal{A}}_c^+ \subseteq \mathcal{A}_c \subseteq \hat{\mathcal{A}}_c^-$ and under similar conditions to the above, $b_k(\hat{\mathcal{A}}_c^\pm) \rightarrow b_k(\mathcal{A}_c)$. Further, in the less general setting where $\mu, \hat{\mu}$ are Morse, if the Hessian of $\hat{\mu}$ converges to that of μ a.s., we conjecture that $m_k(\hat{\mu}) \rightarrow m_k(\mu)$ where m_k is the number of non-degenerate critical points of index k . We propose to submit this theory for publication in the *Journal of Applied and Computational Topology*.

Given Conjecture 1, we propose to derive a partition, $\{V_i\}$, of S such that each V_i properly contains exactly one cluster \mathcal{A}_c (Fig. 4). We denote the i^{th} cluster of \mathcal{A}_c as \mathcal{K}_c^i and define the estimator \mathcal{K}_c^i as $\hat{\mathcal{K}}_c^i := \{s \in V_i : \hat{\mu}(s) \geq c\}$ where $\mathcal{K}_c^i \subseteq \text{Int}(V_i)$, where ‘interior’ is defined respect to the subspace topology on S . Conjecture 1 guarantees that, given enough data $\hat{\mathcal{K}}_c^i$ consist of a single cluster that increasingly resembles \mathcal{K}_c^i . In practical settings, we propose that such a partition may be derived via a support vector machine approach ([16, 34]). The existence of such a $\{V_i\}$ will allow us to treat each cluster in an image in isolation in the following sections.

Feasibility and Risk Management: To derive $\{V_i\}$ in practice, it may be necessary to model the convergence rate of $d_H(\mathcal{A}_c, \hat{\mathcal{A}}_c)$. Inspired by [18], which shows $d_H(\hat{\mathcal{A}}_c, \mathcal{A}_c)$ is a.s. $O(\|\hat{\mu} - \mu\|_\infty)$, preliminary simulations suggest a linear function of $\|\hat{\mu} - \mu\|_\infty$ reliably estimates of $d_H(\hat{\mathcal{A}}_c, \mathcal{A}_c)$ for large n (see Fig. 5). If deriving the exact convergence rate proves intractable, we plan to use extensive fMRI datasets like UKB and HCP to estimate the coefficients for such a fit. Distributional properties of $\|\hat{\mu} - \mu\|_\infty$, and thus $d_H(\hat{\mathcal{A}}, \mathcal{A}_c)$, may then be estimated via standard random field theory ([2, 56]).

Another practical consideration is the use of SVMs to derive the partition $\{V_i\}$, as SVMs can be sensitive to choice of hyperparameters and kernel functions ([8]). We propose to evaluate how such choices impact the generation of $\{V_i\}$ via extensive simulation. Alternative classification methods, such as linear discriminant analysis or perceptron-based approaches, may also be considered to derive decision boundaries ([65, 29]).

2.2 Aim 2: Cluster Size Distribution

In the previous aim, we established that the statistical properties of individual clusters may be studied in isolation. Building on this, we now investigate one of the most fundamental properties of clusters; cluster size. Although many existing methods claim to infer upon *cluster size*, the statements they provide actually concern distribution properties of the *entire excursion set* ([35, 15]). Here, we present the first-ever rigorous statistical treatment of size for individual clusters.

Formally, for an arbitrary set $K \subseteq S$, we define its size as $|K| = \int_{s \in K} \mathbb{1}[s \in K] ds$. For each i , we now aim to derive a CLT for $|\mathcal{K}_c^i|$ in terms of the estimator $|\hat{\mathcal{K}}_c^i|$. By employing the coarea formula from integral geometry and the delta method from probability theory ([24, 59]), we conjecture:

Conjecture 2. Let H_{n-1} be the $(n-1)$ -dimensional Hausdorff measure. If $\nabla \mu$ and $\nabla(\mu|_{\partial S})$ are non-zero on $\partial \mathcal{A}_c$, $\|\hat{\mu}_n - \mu\|_\infty \xrightarrow{d} 0$ and $\|\nabla \hat{\mu}_n - \nabla \mu\|_\infty \xrightarrow{d} 0$, then for each i ;

$$n^{-\frac{1}{2}} (|\hat{\mathcal{K}}_c^i| - |\mathcal{K}_c^i|) \xrightarrow{d} \int_{s \in \partial \mathcal{K}_c^i} \sigma(s) \frac{G(s)}{|\nabla \mu(s)|} dH_{n-1}(s). \quad (4)$$

In practice, we propose to evaluate the expression above numerically by plugging in estimates of $\nabla \mu$, σ and $\partial \mathcal{K}_c^i$, and obtaining samples of $\{G(s)\}_{s \in S}$ via a bootstrapping procedure. The performance of such estimation has been extensively verified in the work [54], [11], [55] and [49]. Notably, in the special case that G is Gaussian, the distribution of the right-hand side is $N(0, \tau^2)$ where τ^2 is the expectation of the squared integral.

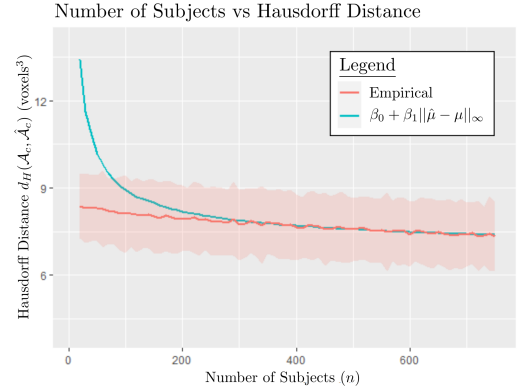


Fig. 5: Empirical estimate of $d_H(\mathcal{A}_c, \hat{\mathcal{A}}_c)$ against sample size (red, with a one-standard-deviation range shaded). Estimated linear fit $\hat{d} = \beta_0 + \beta_1 \|\hat{\mu} - \mu\|_\infty$ (blue). All estimates are derived by averaging over 1000 subsamples, each of sample size n , of the UK Biobank “faces vs shapes” task.

The CLT provided by Conjecture 2 may be employed directly to generate confidence intervals for cluster size and perform cluster size thresholding. Furthermore, by drawing upon results from CR theory, Conjecture 2 may also be used to derive a lower bound for the expected TDP as follows:

Conjecture 3. Denote the empirical TDP for the i^{th} cluster estimate as $TDP(i) = |\hat{\mathcal{K}}_c^i \cap \mathcal{K}_c^i|/|\hat{\mathcal{K}}_c^i|$ and the CDF of $\sup_{\partial\mathcal{A}_c} G_n$ as F . For each i , the below bound holds asymptotically:

$$\mathbb{E}[TDP(i)] \geq \int_0^1 F^{-1} \left[k \left(\int_{s \in \partial\mathcal{K}_c^i} \frac{1}{|\nabla \mu(s)|} dH_{n-1}(s) \right)^{-1} \right] dk$$

Together with Dr. Wouter Weeda of Leiden University, whose recent research centers on fMRI TDP control, we shall compare the performance of the above bound to the methods of [14] and [32] which do not utilize spatial information. We intend to submit the theoretical aspects of this work to *Statistics and Computing*, and applied analyses and implementation to *Neuroimage*, both of which the PI has previously published in ([48, 49]).

Another notable application of Conjecture 2 lies in geostatistical disease prevalence studies where $\hat{\mu}$ is estimated disease prevalence, w is population density, and c is a set threshold. Evaluating integrals of the form $\int_S w(s)\mathbb{P}[\hat{\mu}(s) \geq c]ds$ is pivotal for public health policy formation ([23, 37, 20]). Such analyses may be thought of as estimating the expected value of $w(\hat{\mathcal{A}}_c) := \int_S w(s)\mathbb{1}[\hat{\mu}(s) \geq c]ds$. Noting the similarities between the definitions of $w(\hat{\mathcal{A}}_c)$ and $|\hat{\mathcal{A}}_c|$, Conjecture 2 can be modified to offer a similar CLT for $w(\hat{\mathcal{A}}_c)$.

This observation highlights two key insights: (i) Conjecture 2 enables quantification of the variability in estimating $w(\hat{\mathcal{A}}_c)$, and (ii) the accuracy of this estimation largely depends on the density of sampling near $\partial\mathcal{A}_c$. This latter point has potential to inform targeted sampling strategies in specific geographical zones, increasing both time and cost efficiency.

Feasibility and Risk Management: One risk is the dependency of Conjectures 2 and 3 on the partition $\{V_i\}$ derived in the previous aim. However, in the absence of Aim 1's results, we posit that these conjectures can be reframed to address the entire excursion set, and thus retain much of their value in fMRI and geostatistical settings. Another potential risk is that the proposed methods are based on work that has been extensively verified on fMRI data, but not in the geostatistics setting. A potential obstacle to the proposed application is that the estimation of $F_{\bar{M}}$ via a bootstrapping procedure may not perform as well for irregularly sampled data. To address this, we shall collaborate Prof. Peter Diggle's environmental epidemiology group at the Lancaster Medical School, investigating the performance of alternative resampling methodologies such as those of [19] and [39].

2.3 Aim 3: Spatial Uncertainty for Piecewise Functions

In the previous aims, we constructed a partition of S , $\{V_i\}$, in which each element encompassed a cluster of \mathcal{A}_c . We then formulated cluster size and TDP methods based on $\{V_i\}$. We now adopt the converse approach; starting with an arbitrary partition $\{P_i\}$ of S , we will develop new CR methodology that provides *confidence statements for all partition elements simultaneously, as well as for S as a whole*. We shall then apply this approach to $\{V_i\}$ to produce cluster-specific CRs.

Specifically, we aim to derive CRs for $\mathcal{H} = \{s \in S : h(s) \geq 0\}$ where h , and its estimator \hat{h} , are a.s. piecewise continuous on $\{P_i\}$. Similar to (2), we assume a CLT of the form $\hat{H}_n := \sqrt{n}(\hat{h} - h) \rightarrow H$. However, unlike in (2), H and \hat{H}_n need not be a.s. continuous, only piecewise continuous on $\{P_i\}$. Here, we assume that the convergence is not in the usual distance metric on $C^1(S, \mathbb{R})$, but instead a generalization of the M1 Skorokhod metric, conventionally used to study 1-dimensional discontinuous stochastic processes with unmatched jumps (Fig 7) ([38, 62]). In collaboration with Dr Fabian

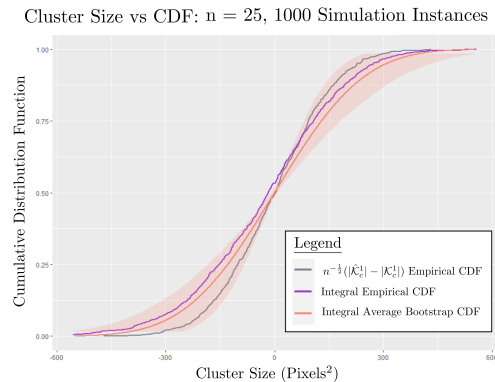


Fig. 6: Simulated empirical CDFs of the left (grey) and right-hand sides (purple) of (4). Also shown is the average bootstrap CDF estimate (pink), with the 95% IQR shaded. In the simulation, μ was a smooth Gaussian bump with peak height 3, $c = 2$ and ϵ was unit Gaussian noise smoothed with FWHM 6.

Telschow from the Humboldt University of Berlin, whose recent research has focused on extending CR methodology, we conjecture the following;

Conjecture 4. Define piecewise CRs $\hat{\mathcal{H}}^\pm := \{s \in S : \hat{h}(s) \geq \pm q/\sqrt{n}\}$, let $\hat{\mathcal{H}}^{i,\pm} := P_i \cap \hat{\mathcal{H}}^\pm$ and $\mathcal{H}^i := P_i \cap \mathcal{H}$. Denote the continuous extension of $H|_{P_i}$ to \bar{P}_i as H^i . Under mild transversality conditions on ∂P_i and $\partial \mathcal{H}$, we have that:

$$(i) \quad \lim_{n \rightarrow \infty} \mathbb{P} \left[\hat{\mathcal{H}}^+ \subseteq \mathcal{H} \subseteq \hat{\mathcal{H}}^- \right] = \mathbb{P} \left[\sup_{s \in \partial \mathcal{H}} |H(s)| < q \right],$$

$$(ii) \quad \forall i, \quad \lim_{n \rightarrow \infty} \mathbb{P} \left[\hat{\mathcal{H}}^{i,+} \subseteq \mathcal{H}^i \subseteq \hat{\mathcal{H}}^{i,-} \right] = \mathbb{P} \left[\sup_{s \in \partial \mathcal{H} \cap P_i} |H^i(s)| \leq q \right].$$

Statement (i) is analogous to (3). However, Statement (ii) provides finer control as it allows for confidence statements to be made for each individual partition element. To be specific, denote $M_i = \sup_{s \in \partial \mathcal{H}_c \cap P_i} |H^i(s)|$, the CDF tail probability of each M_i as F_i , and the joint CDF tail probability of $\bar{\mathbf{M}} = [M_1, \dots, M_n]$ as $F_{\bar{\mathbf{M}}}$. It can be shown that $\varphi(\alpha) := F_{\bar{\mathbf{M}}}^{-1}(\alpha), \dots, F_k^{-1}(\alpha)$ is a non-increasing function of α which can be estimated empirically using $F_{\bar{\mathbf{M}}}$ and $\{F_i\}$. Given a fixed value of β (say $\beta = 5\%$), we propose to find a value of α such that $\varphi(\alpha) = \beta$ via a two-stage bootstrapping procedure. Given such values of α and β , it can be shown that by the definition of φ and Conjecture 4:

$$\text{For each } i, \quad \lim_{n \rightarrow \infty} \mathbb{P} \left[\hat{\mathcal{H}}_c^{i,+} \subseteq \mathcal{H}_c^i \subseteq \hat{\mathcal{H}}_c^{i,-} \right] = 1 - \alpha, \quad \text{and} \quad \lim_{n \rightarrow \infty} \mathbb{P} \left[\hat{\mathcal{H}}_c^+ \subseteq \mathcal{H}_c \subseteq \hat{\mathcal{H}}_c^- \right] = 1 - \beta.$$

This approach allows CRs to be generated for a range of new settings including; partitioned images with potentially mislocalised boundaries, images derived from different sources that have been “stitched” together, and logical combinations of excursion sets such as the set difference (Fig. 8). In the special case that $h := (\mu - c)/\sigma$ and $\{P_i\} = \{V_i\}$, the above method provides cluster-specific CRs with $\alpha\%$ coverage for each cluster individually and $\beta\%$ coverage at the excursion set as a whole. The benefit of the above approach over the original CR method is the guarantee of exact $1 - \alpha$ coverage for each individual cluster separately. Current CR methodology provides no such localization. We intend to submit this work for consideration in the *Journal of the American Statistical Association*.

Feasibility and Risk Management:

A potential obstacle for the two-stage bootstrapping procedure is that the required computation may be infeasible for large datasets. If this proves to be the case, we propose to use dimension-reduction techniques to approximate $\bar{\mathbf{M}}$ ([60, 17]). Further, for testing and evaluation, utilizing parallel processing or distributed computing resources, such as those employed in the PI’s previous work, may also be an option ([47]).

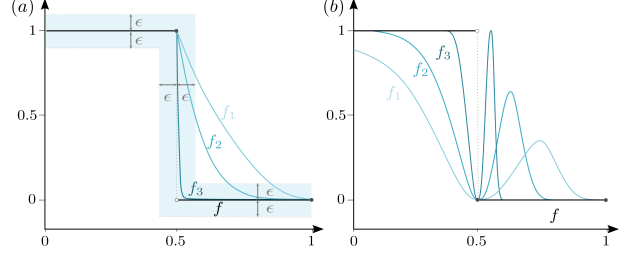


Fig. 7: Pointwise convergent f_n tending to a step function f . In (a), $f_n \xrightarrow{M1^*} f$, whilst in (b), $f_n \not\xrightarrow{M1^*} f$. $M1^*$ convergence ensures that f_n eventually lies inside the shaded blue region shown in (a) and prevents f_n “pinching together” at discontinuities of f such as at $s = 0.5$ in (b).

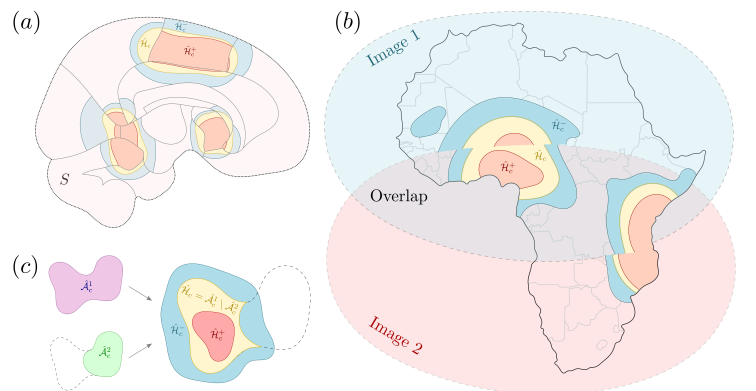


Fig. 8: Example applications of Conjecture 4. (a) Piecewise CRs for fMRI atlases, providing simultaneous confidence statements for each brain region, as well as the entire brain. (b) CRs for combined images; with simultaneous statements made for both images, their overlap and union. (c) CRs for the set difference; confidence statements are made about the activation present in one image ($\hat{\mathcal{A}}_c^1$) but not another ($\hat{\mathcal{A}}_c^2$).

3 Project Plan

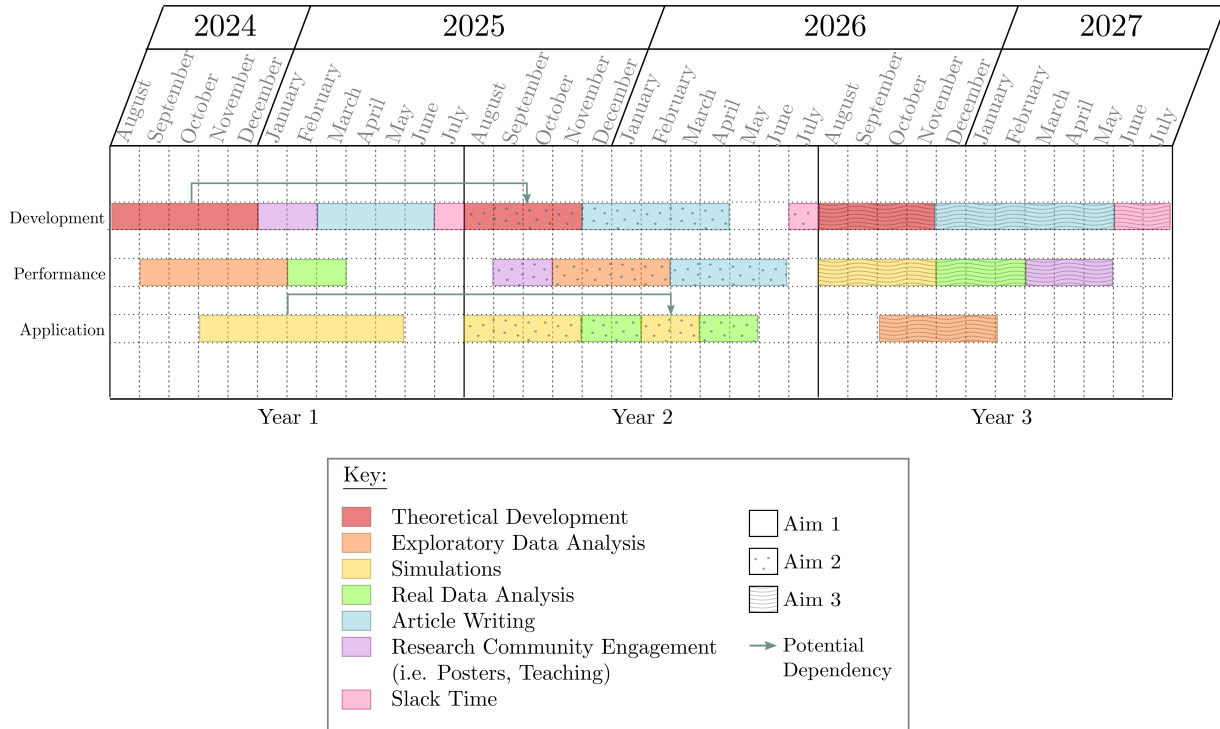


Fig. 9: Gantt chart of the proposed project timeline. Three primary workflows are depicted: Development (focused on theoretical and presentational tasks), Performance (rigorously assessing methodological capability), and Application (exploring real-world hypotheses with large datasets). Task distinctions are color-coded, aims are textured, and dependencies are marked with arrows.

References

- [1] R. J. Adler. *The geometry of random fields*. Wiley series in probability and mathematical statistics. Probability and mathematical statistics. J. Wiley, 1981. DOI: 10.1137/1.9780898718980.
- [2] R. J. Adler, K. Bartz, S. C. Kou, and A. Monod. *Estimating thresholding levels for random fields via Euler characteristics*. 2017. DOI: 10.48550/arXiv.1704.08562.
- [3] R. J. Adler and S. K. Iyer. “Attractive polymer models for two- and three-dimensional Brownian motion”. *Stochastic Processes and their Applications* 66.2 (1997), pp. 271–281. DOI: 10.1016/S0304-4149(96)00126-3.
- [4] R. J. Adler and J. Taylor. *Random Fields and Geometry*. Springer Monographs in Mathematics. Springer New York, 2009.
- [5] N. Allen et al. “UK Biobank: Current status and what it means for epidemiology”. *Health Policy and Technology* 1.3 (2012), pp. 123 –126. DOI: 10.1016/j.hlpt.2012.07.003.
- [6] J. Azais and M. Wschebor. *Level Sets and Extrema of Random Processes and Fields*. Wiley, 2009. DOI: 10.1002/9780470434642.
- [7] S. Basodi et al. “Decentralized Mixed Effects Modeling in COINSTAC”. *bioRxiv* (2023). DOI: 10.1101/2023.05.12.540598.
- [8] K. P. Bennett and C. Campbell. “Support Vector Machines: Hype or Hallelujah?” *SIGKDD Explor. Newsl.* 2.2 (Dec. 2000), 1–13. DOI: 10.1145/380995.380999.
- [9] A. Blain, B. Thirion, and P. Neuvial. “Notip: Non-parametric true discovery proportion control for brain imaging”. *NeuroImage* 260 (2022), p. 119492. DOI: 10.1016/j.neuroimage.2022.119492.
- [10] D. Bolin and F. Lindgren. “Excursion and contour uncertainty regions for latent Gaussian models”. *Journal of the Royal Statistical Society. Series B (Statistical Methodology)* 77.1 (2015), pp. 85–106. DOI: 10.1111/rssb.12055. (Visited on 04/20/2022).
- [11] A. Bowring, F. Telschow, A. Schwartzman, and T. E. Nichols. “Spatial confidence sets for raw effect size images”. *NeuroImage* 203 (2019), p. 116187. DOI: 10.1016/j.neuroimage.2019.116187.
- [12] A. Bowring, F. J. Telschow, A. Schwartzman, and T. E. Nichols. “Confidence Sets for Cohen’s d effect size images”. *NeuroImage* 226 (2021), p. 117477. DOI: 10.1016/j.neuroimage.2020.117477.
- [13] J. Cao and K. J. Worsley. “The detection of local shape changes via the geometry of Hotelling’s T^2 fields”. *The Annals of Statistics* 27.3 (1999), pp. 925 –942. DOI: 10.1214/aos/1018031263.
- [14] X. Chen et al. *Adaptive Cluster Thresholding with Spatial Activation Guarantees Using All-resolutions Inference*. 2023. DOI: 10.48550/arXiv.2206.13587.
- [15] Y.-C. Chen, C. R. Genovese, and L. Wasserman. “Density Level Sets: Asymptotics, Inference, and Visualization”. *Journal of the American Statistical Association* 112.520 (2017), pp. 1684–1696. DOI: 10.1080/01621459.2016.1228536.
- [16] N. Christianini and J. Shawe-Taylor. *An Introduction to Support Vector Machines and Other Kernel-Based Learning Methods*. Cambridge, UK: Cambridge University Press, 2000. DOI: 10.1017/CBO9780511801389.
- [17] B. R. Conroy, J. M. Walz, and P. Sajda. “Fast Bootstrapping and Permutation Testing for Assessing Reproducibility and Interpretability of Multivariate fMRI Decoding Models”. *PLOS ONE* 8.11 (Nov. 2013), pp. 1–11. DOI: 10.1371/journal.pone.0079271. URL: 10.1371/journal.pone.0079271.
- [18] A. Cuevas, W. González-Manteiga, and A. Rodríguez-Casal. “Plug-in estimation of general level sets”. *Australian & New Zealand Journal of Statistics* 48.1 (2006), pp. 7–19. DOI: 10.1111/j.1467-842X.2006.00421.x.

- [19] C. V. Deutsch. *A statistical resampling program for correlated data: spatial_bootstrap*. Tech. rep. University of Alberta, Edmonton, Canada: Centre for Computational Geostatistics Annual Report, 2004. URL: http://ccgalberta.com/ccgresources/report06/2004-401-spatial_bootstrap.pdf.
- [20] P. J. Diggle et al. *Modernising the Design and Analysis of Prevalence Surveys for Neglected Tropical Diseases*. 2023. DOI: 10.1098/rstb.2022.0276.
- [21] H. Edelsbrunner and J. Harer. *Computational Topology: An Introduction*. Miscellaneous Bks. American Mathematical Society, 2022. DOI: 10.1007/978-3-540-33259-6_7.
- [22] A. Eklund, T. E. Nichols, and H. Knutsson. “Cluster failure: Why fMRI inferences for spatial extent have inflated false-positive rates”. *Proceedings of the national academy of sciences* 113.28 (2016), pp. 7900–7905. DOI: 10.1073/pnas.1602413113.
- [23] *Ending the neglect to attain the Sustainable Development Goals: a framework for monitoring and evaluating progress of the road map for neglected tropical diseases 2021-2030*. World Health Organization, 2020. URL: <https://books.google.co.uk/books?id=TMJqEAAAQBAJ>.
- [24] H. Federer. *Geometric Measure Theory*. Classics in Mathematics. Springer Berlin Heidelberg, 2014. DOI: 10.1007/978-3-642-62010-2.
- [25] K. J. Friston et al. “Assessing the significance of focal activations using their spatial extent”. *Human Brain Mapping* 1.3 (1994), pp. 210–220. DOI: 10.1002/hbm.460010306.
- [26] K. J. Friston et al. “Statistical parametric maps in functional imaging: A general linear approach”. *Human Brain Mapping* 2.4 (1995), pp. 189–210. DOI: 10.1002/hbm.460020402.
- [27] K. Friston et al. “Detecting Activations in PET and fMRI: Levels of Inference and Power”. *NeuroImage* 4.3 (1996), pp. 223–235. DOI: 10.1006/nimg.1996.0074.
- [28] J. Gaite. “The Fractal Geometry of the Cosmic Web and Its Formation”. *Advances in Astronomy* 2019 (May 2019), p. 6587138. DOI: 10.1155/2019/6587138.
- [29] S. Gallant. “Perceptron-based learning algorithms”. *IEEE Transactions on Neural Networks* 1.2 (1990), pp. 179–191. DOI: 10.1109/72.80230.
- [30] C. R. Genovese, N. A. Lazar, and T. Nichols. “Thresholding of Statistical Maps in Functional Neuroimaging Using the False Discovery Rate”. *NeuroImage* 15.4 (2002), pp. 870–878. DOI: 10.1006/nimg.2001.1037.
- [31] E. Giorgi et al. “Model building and assessment of the impact of covariates for disease prevalence mapping in low-resource settings: to explain and to predict”. *Journal of The Royal Society Interface* 18.179 (2021), p. 20210104. DOI: 10.1098/rsif.2021.0104.
- [32] J. J. Goeman et al. “Cluster extent inference revisited: quantification and localisation of brain activity”. *Journal of the Royal Statistical Society Series B: Statistical Methodology* (July 2023), qkad067. DOI: 10.1093/rsssb/qkad067.
- [33] B. Guillaume, T. Nichols, and T. Maullin-Sapey. *Sandwich Estimator toolbox code*. 2018. URL: <https://github.com/NIS0x-BDI/SwE-toolbox> (Accessed: 19/08/2018).
- [34] T. Hastie, R. Tibshirani, and J. Friedman. *The Elements of Statistical Learning*. 2nd ed. New York: Springer, 2008. DOI: 10.1007/978-0-387-84858-7.
- [35] S. Hayasaka et al. “Nonstationary cluster-size inference with random field and permutation methods”. *NeuroImage* 22.2 (2004), pp. 676–687. DOI: 10.1016/j.neuroimage.2004.01.041.
- [36] R. Heller et al. “Cluster-based analysis of fMRI data”. *NeuroImage* 33.2 (2006), pp. 599–608. DOI: 10.1016/j.neuroimage.2006.04.233.
- [37] O Johnson et al. “Model-Based Geostatistical Methods Enable Efficient Design and Analysis of Prevalence Surveys for Soil-Transmitted Helminth Infection and Other Neglected Tropical Diseases”. *Clin Infect Dis* 72.Suppl 3 (June 2021), S172–S179. DOI: 10.1093/cid/ciab192.
- [38] J. Kern. *The Skorokhod Topologies: What They Are and Why We Should Care*. 2022. DOI: 10.48550/arXiv.2210.16026.

- [39] K. D. Khan and C. V. Deutsch. "Practical Incorporation of Multivariate Parameter Uncertainty in Geostatistical Resource Modeling". *Natural Resources Research* 25.1 (Mar. 2016), pp. 51–70. DOI: 10.1007/s11053-015-9267-y.
- [40] E. Mammen and W. Polonik. "Confidence regions for level sets". *Journal of Multivariate Analysis* 122 (2013), pp. 202–214. DOI: 10.1016/j.jmva.2013.07.017.
- [41] T. Maullin-Sapey, C. Maumet, and T. Nichols. "Detecting and Interpreting Heterogeneity and Publication Bias in Image-Based Meta Analyses". *OHBM Conference Poster*. 2018. DOI: 10.6084/m9.figshare.21842349.v1.
- [42] T. Maullin-Sapey and T. Nichols. "BLMM: Parallelised Computing for Big Linear Mixed Models". *SMI Conference Poster*. 2021. DOI: 10.6084/m9.figshare.21842097.v1.
- [43] T. Maullin-Sapey, A. Schwartzman, and T. Nichols. "Spatial Confidence Regions for Conjunctions of fMRI Effects". *OHBM & RSS Conference Poster*. 2022. DOI: 10.6084/m9.figshare.21836901.v1.
- [44] T. Maullin-Sapey. *Big Linear Mixed Models code*. 2021. URL: <https://github.com/TomMaullin/BLMM/tree/master/BLMM> (Accessed: 10/09/2023).
- [45] T. Maullin-Sapey. *Big Linear Models code*. 2019. URL: <https://github.com/TomMaullin/BLM/tree/master/BLM> (Accessed: 20/02/2020).
- [46] T. Maullin-Sapey. *Confidence Regions Toolbox code*. 2023. URL: <https://github.com/TomMaullin/crtoolbox/tree/master/crtoolbox> (Accessed: 10/09/2023).
- [47] T. Maullin-Sapey and T. E. Nichols. "BLMM: Parallelised computing for big linear mixed models". *NeuroImage* 264 (2022), p. 119729. DOI: 10.1016/j.neuroimage.2022.119729.
- [48] T. Maullin-Sapey and T. E. Nichols. "Fisher Scoring for crossed factor linear mixed models". *Statistics and Computing* 31.5 (2021), p. 53. DOI: 10.1007/s11222-021-10026-6.
- [49] T. Maullin-Sapey, A. Schwartzman, and T. E. Nichols. "Spatial Confidence Regions for Combinations of Excursion Sets in Image Analysis". *arXiv:2201.02743* (2022). DOI: 10.48550/arXiv.2201.02743.
- [50] C. Maumet and T. Maullin-Sapey. *Image Based Meta Analysis code*. 2017. URL: <https://github.com/TomMaullin/ibma> (Accessed: 19/06/2017).
- [51] N. Paquette et al. "Ventricular shape and relative position abnormalities in preterm neonates". *NeuroImage: Clinical* 15 (2017), pp. 483–493. DOI: 10.1016/j.nicl.2017.05.025.
- [52] E. Proal et al. "Brain gray matter deficits at 33-year follow-up in adults with attention-deficit /hyperactivity disorder established in childhood". *Archives of general psychiatry* 68.11 (2011), pp. 1122–1134. DOI: 10.1001/archgenpsychiatry.2011.117.
- [53] S. M. Smith and T. E. Nichols. "Threshold-free cluster enhancement: addressing problems of smoothing, threshold dependence and localisation in cluster inference". en. *NeuroImage* 44.1 (Jan. 2009), pp. 83–98. DOI: 10.1016/j.neuroimage.2008.03.061.
- [54] M. Sommerfeld, S. Sain, and A. Schwartzman. "Confidence Regions for Spatial Excursion Sets From Repeated Random Field Observations, With an Application to Climate". *Journal of the American Statistical Association* 113.523 (2018). PMID: 31452557, pp. 1327–1340. DOI: 10.1080/01621459.2017.1341838.
- [55] F. Telschow and A. Schwartzman. "Simultaneous confidence bands for functional data using the Gaussian Kinematic formula". *Journal of Statistical Planning and Inference* 216 (June 2021). DOI: 10.1016/j.jspi.2021.05.008.
- [56] F. Telschow, A. Schwartzman, D. Cheng, and P. Pranav. *Estimation of Expected Euler Characteristic Curves of Nonstationary Smooth Gaussian Random Fields*. 2020. DOI: 10.48550/arXiv.1908.02493.
- [57] The NIDASH group. *NIDM Results viewer code*. 2017. URL: <https://github.com/ncf-nidash/nidmresults-fslhtml> (Accessed: 09/09/2017).

- [58] A. Topiwala, K. Ebmeier, T. Maullin-Sapey, and T. Nichols. “Alcohol consumption and MRI markers of brain structure and function: Cohort study of 25,378 UK Biobank participants”. *NeuroImage: Clinical* 35 (2022), p. 103066. DOI: <https://doi.org/10.1016/j.nicl.2022.103066>.
- [59] A. van der Vaart and J. Wellner. *Weak Convergence and Empirical Processes: With Applications to Statistics*. Springer Series in Statistics. Springer, 1996. DOI: 10.1007/978-3-031-29040-4.
- [60] S. Van Aelst and G. Willems. “Fast and Robust Bootstrap for Multivariate Inference: The R Package FRB”. *Journal of Statistical Software* 53.3 (2013), 1–32. DOI: 10.18637/jss.v053.i03.
- [61] D. Van Essen et al. “The WU-Minn Human Connectome Project: an overview”. *NeuroImage* 80 (May 2013). DOI: 10.1016/j.neuroimage.2013.05.041.
- [62] W. Whitt. *Stochastic-Process Limits: An Introduction to Stochastic-Process Limits and Their Application to Queues*. Springer Series in Operations Research and Financial Engineering. Springer New York, 2002. URL: <https://books.google.co.uk/books?id=imq84GrwDLYC>.
- [63] C.-W. Woo, A. Krishnan, and T. D. Wager. “Cluster-extent based thresholding in fMRI analyses: Pitfalls and recommendations”. *NeuroImage* 91 (2014), pp. 412–419. DOI: 10.1016/j.neuroimage.2013.12.058.
- [64] K. J. Worsley. “The Geometry of Random Images”. *CHANCE* 9.1 (1996), pp. 27–40. DOI: 10.1080/09332480.1996.10542483.
- [65] P. Xanthopoulos, P. M. Pardalos, and T. B. Trafalis. “Linear Discriminant Analysis”. *Robust Data Mining*. New York, NY: Springer New York, 2013, pp. 27–33. DOI: 10.1007/978-1-4419-9878-1_4.
- [66] H. Zhang, T. E. Nichols, and T. D. Johnson. “Cluster mass inference via random field theory”. *NeuroImage* 44 (2009), pp. 51–61. DOI: 10.1016/j.neuroimage.2008.08.017.